

## Electronic supplementary information (ESI)

### **Constructing TiO<sub>2</sub>@MOF S-scheme heterojunctions for enhanced photocatalytic degradation of antibiotic and Cr(VI) photoreduction**

Yuqi Wan,<sup>a,b</sup> Ke Gao,<sup>a</sup> Zhiquan Pan,<sup>a</sup> Tianshuo Zhao,<sup>b\*</sup> and Qingrong Cheng,<sup>a\*</sup>

<sup>a</sup> School of Chemistry and Environmental Engineering, Wuhan Institute of Technology, Wuhan, 430205, China.

<sup>b</sup> Department of Electrical and Electronic Engineering, The University of Hong Kong, Hong Kong SAR, China.

## Contents:

- Text S1** Photocatalytic experiments for Cr(VI) reduction
- Table S1** Crystallographic data for the complex
- Table S2** Selected bond distances (Å) and angles (°) for the complex
- Table S3** Specific surface areas, pore volume and mean pore diameters for P-TiO<sub>2</sub> and Zn-MOF<sub>0.5</sub>/P-TiO<sub>2</sub>
- Table S4** Comparison of the CIP reduction capacity of P-TiO<sub>2</sub>/Zn-MOF<sub>2.0</sub> with other photocatalysts
- Table S5** Comparison of the Cr(VI) reduction capacity of P-TiO<sub>2</sub>/Zn-MOF<sub>2.0</sub> with other photocatalysts
- Table S6** Ion contents and properties of raw electroplating wastewater
- Table S7** The fitted parameters obtained from decay curves of the samples
- Table S8** Comparison of calculation results and experimental results of VBM and CBM of materials
- Figure S1** The structural unit of 44-membered ring
- Figure S2** PXRD pattern and simulated pattern of Zn-MOF
- Figure S3** (a) N<sub>2</sub> absorption isotherms of P-TiO<sub>2</sub> and P-TiO<sub>2</sub>@Zn-MOF<sub>2.0</sub>; (b) the particle size distribution obtained by NLDFT kernel
- Figure S4** Zn (a) and O1s (b) XPS spectrum of P-TiO<sub>2</sub>@Zn-MOF<sub>2.0</sub>
- Figure S5** The band gap energy of P-TiO<sub>2</sub>@Zn-MOF<sub>2.5</sub>
- Figure S6** Photocatalytic CIP degradation during four consecutive runs of P-TiO<sub>2</sub>@Zn-MOF<sub>2.0</sub>(a); The PXRD patterns for P-TiO<sub>2</sub>@Zn-MOF<sub>2.0</sub> before and after CIP degradation(b)
- Figure S7** The mass spectra of intermediates during CIP degradation
- Figure S8** The transformation pathways of product F from CIP
- Figure S9** The photocatalytic degradation of TC by the different catalysts
- Figure S10** Kinetics curves of photocatalytic reduction of Cr(VI) for P-TiO<sub>2</sub>@Zn-MOF<sub>2.0</sub> at different conditions
- Figure S11** Photocatalytic reduction of Cr(VI) over P-TiO<sub>2</sub>@Zn-MOF<sub>2.0</sub> with or without electron scavenger of K<sub>2</sub>S<sub>2</sub>O<sub>8</sub> (0.1 mmol)
- Figure S12** PXRD patterns of P-TiO<sub>2</sub>@Zn-MOF<sub>2.0</sub> before and after soaking in acid for 72 hours and 7 days, respectively

**Figure S13** The time-dependent Cr(VI) photoreduction efficiency of P-TiO<sub>2</sub>@Zn-MOF<sub>2.0</sub> in the electroplating waste water (pH = 1.98)

**Figure S14** PXRD of P-TiO<sub>2</sub>@Zn-MOF<sub>2.0</sub> after 8 runs

**Figure S15** The fitted decay curves of P-TiO<sub>2</sub> (a) and P-TiO<sub>2</sub>@Zn-MOF<sub>2.0</sub>(b)

### Text S1: Photocatalytic experiments for Cr(VI) reduction

The photocatalytic experiments for aqueous Cr(VI) to Cr(III) were carried out under 300 W Xe irradiation at ambient conditions in a 150 mL quartz reactor containing 20.0 mg photocatalysts which were dispersed into 100 mL of a Cr(VI) aqueous solution (10.0 ppm). Prior to irradiation, the suspension was magnetically stirred for 60 min in the dark to ensure an adsorption–desorption equilibrium and then different volumes of 0.2 M H<sub>2</sub>SO<sub>4</sub> were added to adjust the acidity in the reaction, with the pH values determined using a pH detector. During the reduction of aqueous Cr(VI), stirring was maintained to keep the mixture in suspension, 2.0 mL of suspension was withdrawn at regular intervals and the photocatalyst was separated by centrifugation. Then, the Cr(VI) content in the solution was determined colorimetrically by the diphenylcarbazide method (DPC) with a detection limit of 0.005 mg L<sup>-1</sup>. The Cr(VI) content in the solution at different illumination times was monitored by measuring its maximum absorbance (centered at 540 nm) using a UV visible spectrophotometer.

**Table S1** Crystallographic data for Zn-MOF.

Empirical formula	C <sub>10</sub> H <sub>14</sub> O <sub>6</sub> P <sub>2</sub> Zn	Formula weight	357.52
Crystal system	monoclinic	Space group	P 1 21/c 1 (14)
a (Å)	4.5297(5)	b (Å)	19.0682(19)
c (Å)	14.6610(15)	α (deg)	90
β(deg)	96.314(4)	γ (deg)	90
Volume (Å <sup>3</sup> )	1258.64(20)	Z	4
D (calc) (g cm <sup>-3</sup> )	1.88661	Mu(Mo-Ka)[mm <sup>-1</sup> ]	
F(000)	728	H,k,l max	4, 22, 16
Temp , k	173(2)	Nref,Npar	2043, 174
R, wR <sub>2</sub>	0.1152, 0.1287	S	1.044

**Table S2** Selected bond distances (Å) and angles (°) for Zn-MOF.

bond lengths(Å)		bond lengths(Å)	
Zn1- O1	2.147(5)	O1- Zn1	2.015(5)
O3- Zn1	2.128(5)	O5- Zn1	1.984(5)
O6- Zn1	1.928(6)	O6- Zn1- O1	128.6(2)
O6- Zn1- O5	102.1(2)	O6- Zn1- O3	91.7(2)
O5- Zn1- O1	129.2(2)	O1- Zn1- O3	90.6(2)
O5- Zn1- O3	90.2(2)	O5- Zn1- O1	100.1(2)
O6- Zn1- O1	91.6(2)	O3- Zn1- O1	168.3(2)
O1- Zn1- O1	78.6(2)		

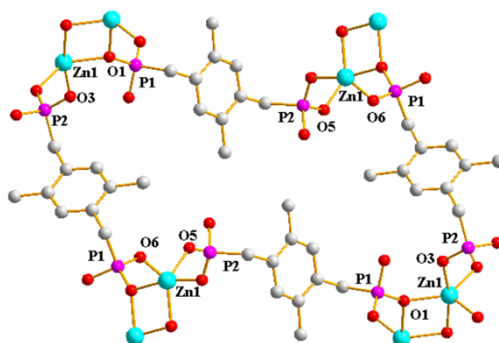


**Fig.S1** The structural unit of 44-membered ring.

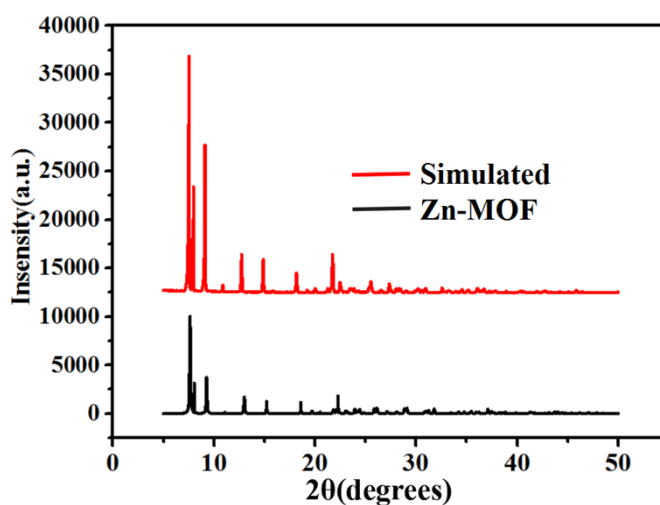


**Fig.S2** PXRD pattern and simulated pattern of Zn-MOF.

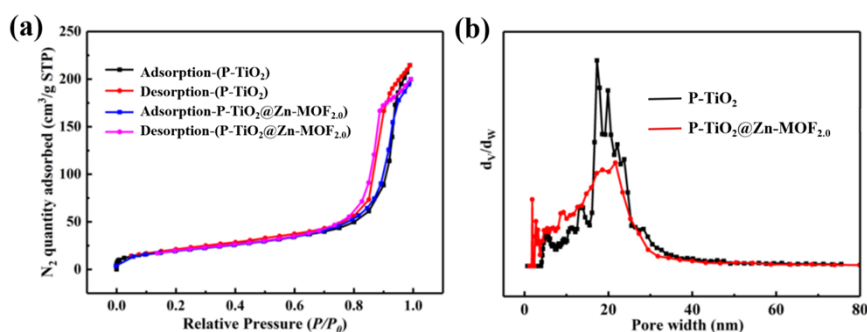


**Fig.S3** (a)  $N_2$  absorption isotherms of P-TiO<sub>2</sub> and P-TiO<sub>2</sub>@Zn-MOF<sub>2.0</sub>; (b) the particle size distribution obtained by NLDFT kernel.

**Table S3** Specific surface areas, pore volume and mean pore diameters for P-TiO<sub>2</sub> and P-TiO<sub>2</sub>@Zn-MOF<sub>2.0</sub>.

Materials	$S_{BET}$ (m <sup>2</sup> /g)	Pore volume (cm <sup>3</sup> /g)	Average diameter of mesoporous (nm)
P-TiO <sub>2</sub>	74.16	0.3326	17.94
P-TiO <sub>2</sub> @Zn-MOF <sub>2.0</sub>	71.06	0.3089	14.53

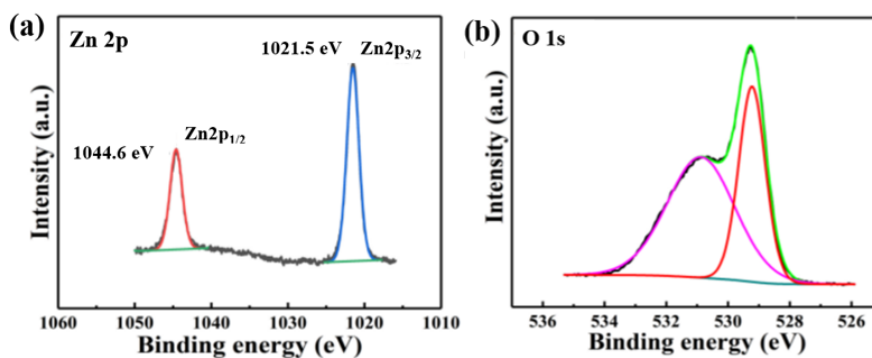


**Fig.S4** Zn (a) and O1s (b) XPS spectrum of P-TiO<sub>2</sub>@Zn-MOF<sub>2.0</sub>.

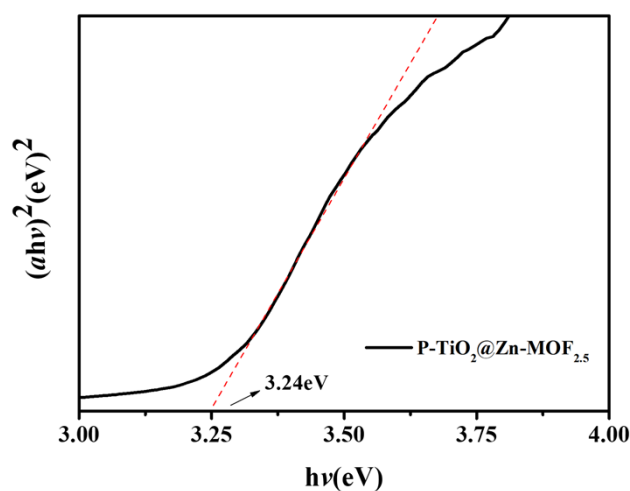


**Fig. S5** The band gap energy of P-TiO<sub>2</sub>@Zn-MOF<sub>2.5</sub>.

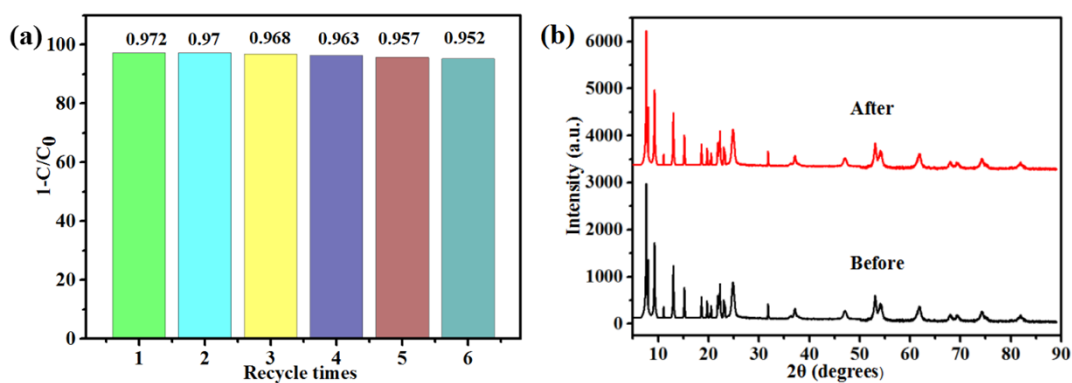


**Fig. S6** Photocatalytic CIP degradation during six consecutive runs of P-TiO<sub>2</sub>@Zn-MOF<sub>2.0</sub>(a); The PXRD patterns for P-TiO<sub>2</sub>@Zn-MOF<sub>2.0</sub> before and after CIP degradation(b).

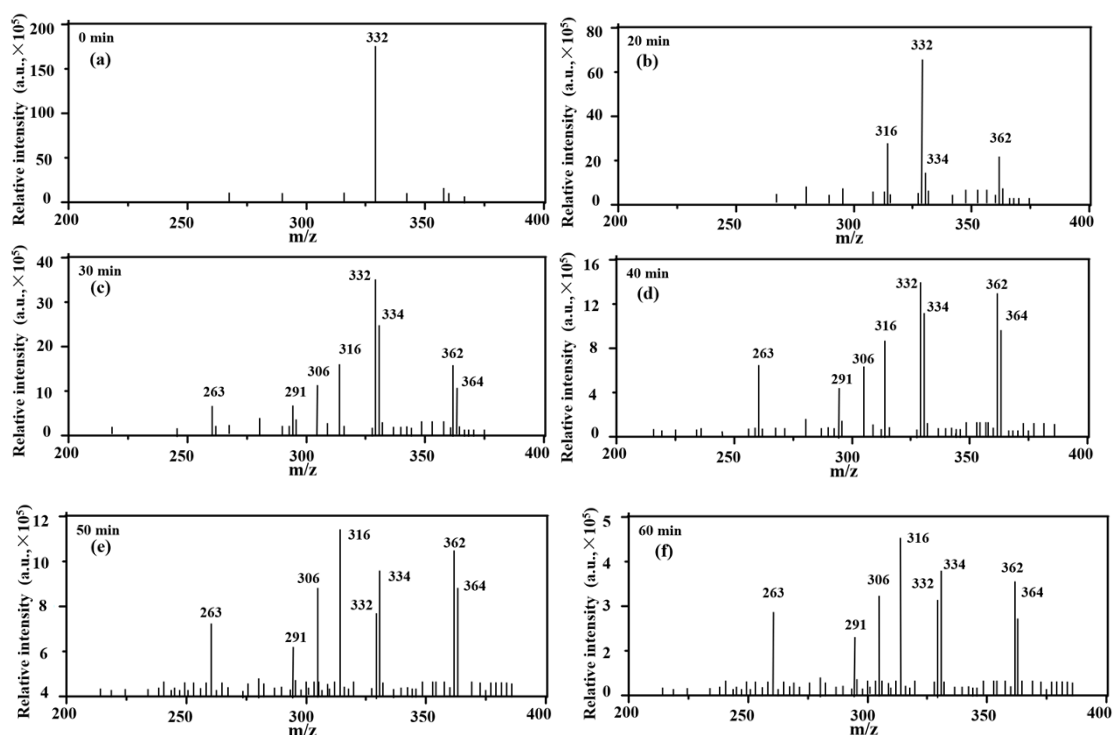


**Fig. S7** The mass spectra of intermediates during CIP degradation.

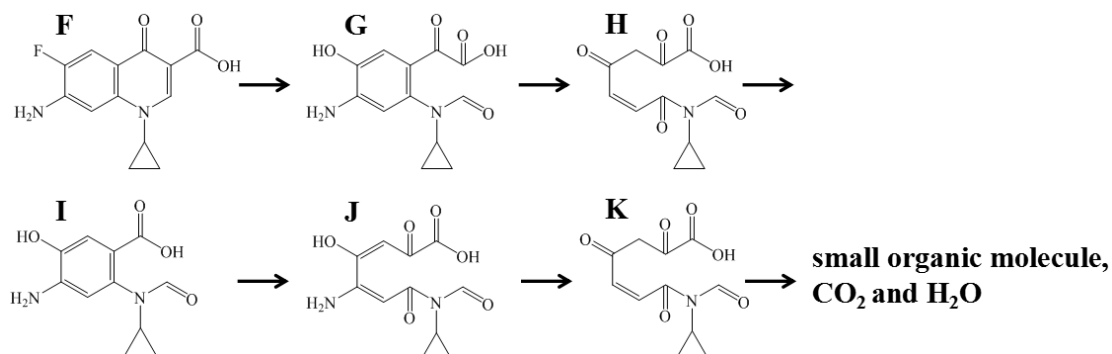


**Fig. S8** The transformation pathways of product F from CIP.

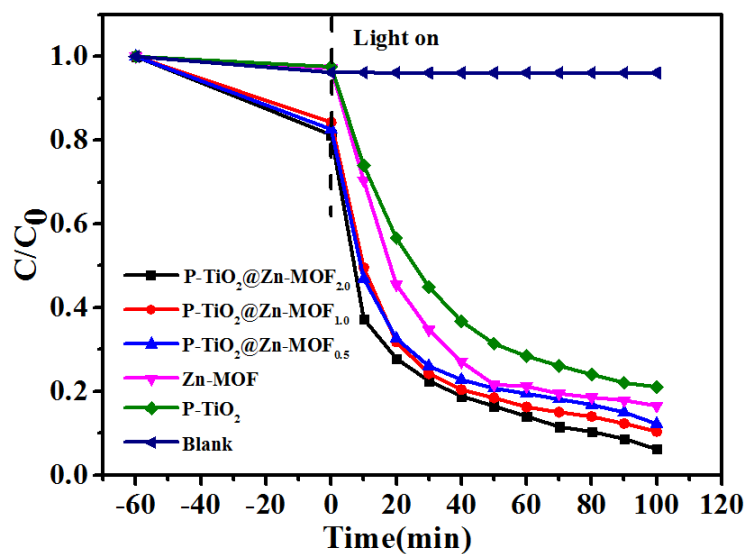


Fig. S9 The photocatalytic degradation of TC by different catalysts.

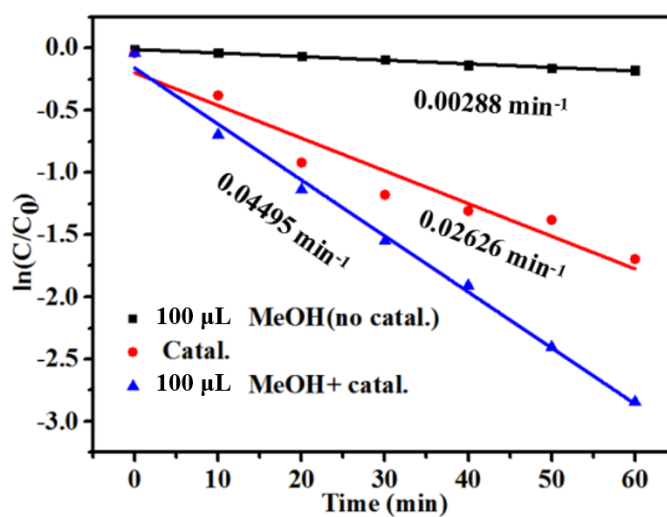
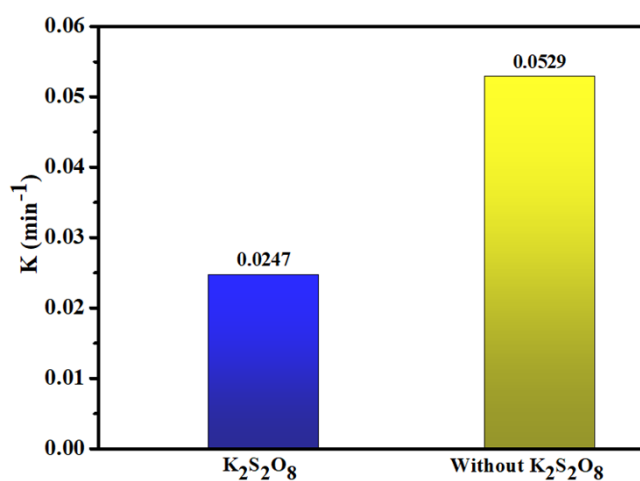
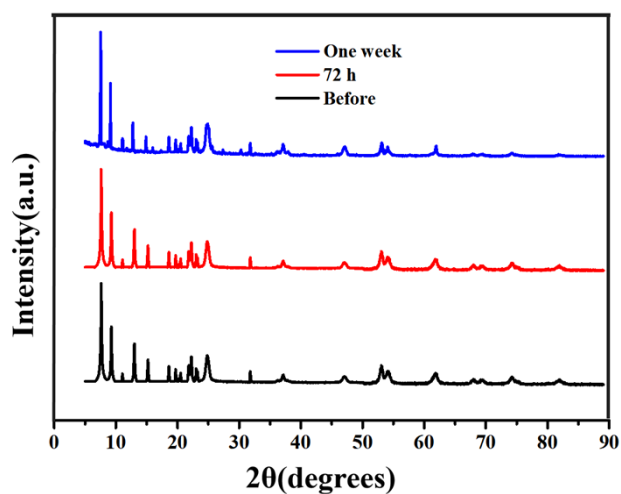


Fig. S10 Kinetics curves of photocatalytic reduction of Cr(VI) for P-TiO<sub>2</sub>@Zn-MOF<sub>2.0</sub> at different conditions.





**Fig. S11** Photocatalytic reduction of Cr(VI) over P-TiO<sub>2</sub>@Zn-MOF<sub>2.0</sub> with or without electron scavenger of K<sub>2</sub>S<sub>2</sub>O<sub>8</sub> (0.1 mmol).



**Fig. S12** PXRD patterns of P-TiO<sub>2</sub>@Zn-MOF<sub>2.0</sub> before and after immersing in acid for 72 hours and 7 days, respectively.

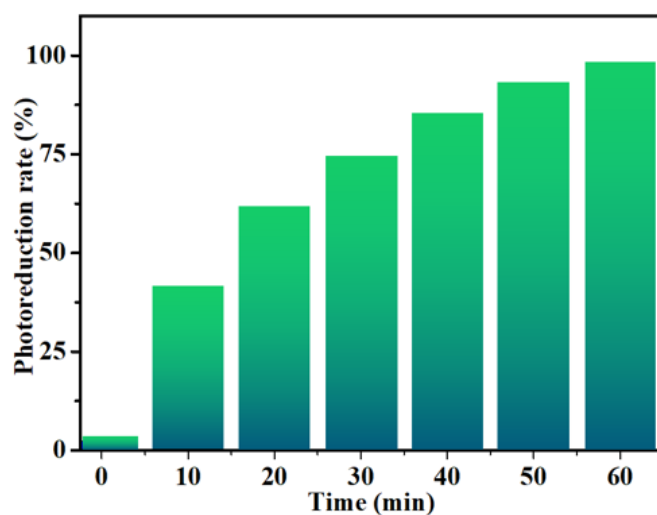


**Fig. S13** The time-dependent Cr(VI) photoreduction efficiency of P-TiO<sub>2</sub>@Zn-MOF<sub>2.0</sub> in the electroplating waste water (pH = 1.98)

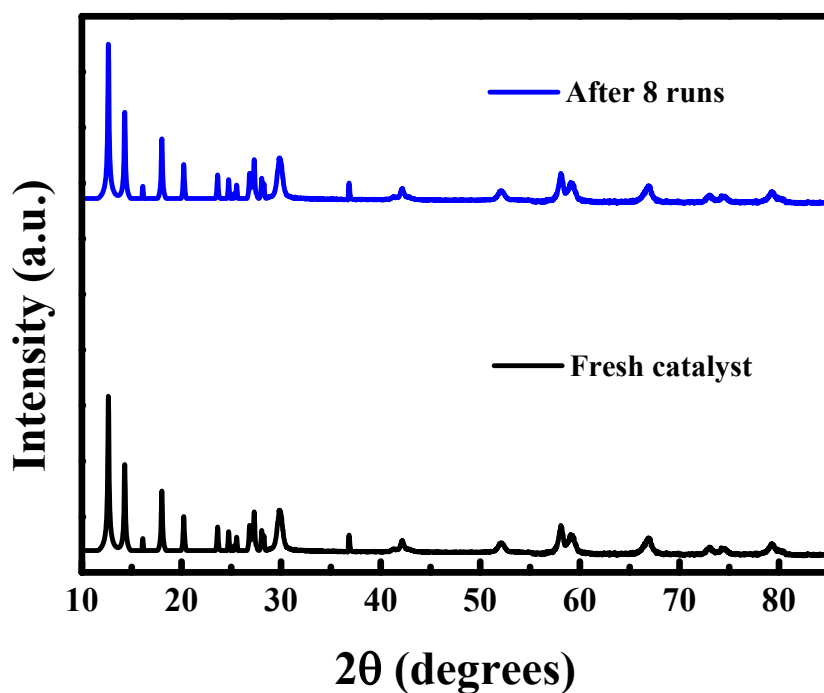


Fig. S14 PXRD of P-TiO<sub>2</sub>@Zn-MOF<sub>2.0</sub> after 8 runs.

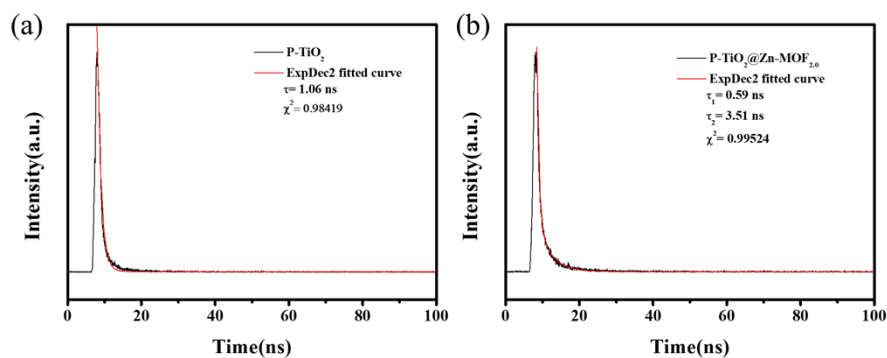


Fig. S15 The fitted decay curves of P-TiO<sub>2</sub> (a) and P-TiO<sub>2</sub>@Zn-MOF<sub>2.0</sub> (b)

**Table S4** Comparison of the CIP reduction capacity of P-TiO<sub>2</sub>@Zn-MOF<sub>2.0</sub> with other photocatalysts.

Catalyst/mg	V (mL)/ C <sub>0</sub> (mg L <sup>-1</sup> )	Light source	Time (min)	Result (%)	K (min <sup>-1</sup> )	Ref.
P-TiO <sub>2</sub> /Zn-MOF <sub>2.0</sub> /20	100/10	300 W Xe lamp	60	97.2	0.023	This work
MOF-derived C-TiO <sub>2</sub> /50	100/10	300 W Xe lamp	120	72.4	0.0085	[1]
Bi <sub>2</sub> MoO <sub>6</sub> /GQDs/TiO <sub>2</sub>	5/10	300 W Xe lamp	150	90.21	0.015	[2]
Vo-TiO <sub>2</sub> /Ta <sub>3</sub> N <sub>5</sub> -3 /50	50/10	300 W Xe lamp	90	95.7	0.0249	[3]
CTH-0.5/80	100/15	300 W Xe lamp	60	87	/	[4]

**Table S5** Comparison of the Cr(VI) reduction capacity of P-TiO<sub>2</sub>/Zn-MOF<sub>2.0</sub> with other photocatalysts.

Catalyst/mg	V (mL)/ C <sub>0</sub> (mg L <sup>-1</sup> )/pH	Light source	Time (min)	Result (%)	K (min <sup>-1</sup> )	Ref.
P-TiO <sub>2</sub> /Zn-MOF <sub>2.0</sub> /20	100/10/1.98	300 W Xe lamp	60	92.8	0.045	This work
CuAl <sub>2</sub> O <sub>4</sub> /TiO <sub>2</sub>	60/30/2.0	200 W tungsten	180	95	0.016	[5]
10Ag@C-TCZ/50	100/5/3.0	500 W Xe lamp	120	95.5	/	[6]
0.2CDs-TNs <sup>a</sup> /50	50/10/3.0	500 W Xe lamp	120	99.2 <sup>a</sup>	0.027	[7]
GO/TiO <sub>2</sub> <sup>b</sup> /500	1000/10/2.0	8 W Hg lamp	420	99.6 <sup>b</sup>	0.4228	[8]
MIL-125(Ti)-derived COOH	200/5/2.0	/	90	61.8	/	[9]

<sup>a</sup> CDs-TNs = carbon dots-TiO<sub>2</sub> nanosheets. <sup>b</sup> GO/TiO<sub>2</sub> = a graphene oxide@TiO<sub>2</sub> composite.

**Table S6** Ion contents and properties of raw electroplating wastewater.

item	concentration (mg/L)	item	concentration(mg/L)
pH value	1.98	Ca <sup>2+</sup>	35.83
TOC	98.72	Ba <sup>2+</sup>	76.01
Cr(VI)	102.48	SO <sub>4</sub> <sup>2-</sup>	653.31
Na <sup>+</sup>	61.63	NO <sub>3</sub> <sup>-</sup>	1501.42
K <sup>+</sup>	25.68		

**Table S7** The fitted parameters obtained from decay curves of the samples

Sample	E <sub>w</sub>	τ <sub>1</sub> (ns)	τ <sub>2</sub> (ns)	χ <sup>2</sup>
P-TiO <sub>2</sub>	350 nm	1.0585	-	0.98419
P-TiO <sub>2</sub> @Zn-MOF <sub>2.0</sub>	350 nm	0.5893	3.5054	0.99524

**Table S8** Comparison of calculation results and experimental results of VBM and CBM of materials.

Zn-MOF	VBM vs. NHE (eV)	CBM vs. NHE (eV)
Calculation results	3.84	-0.20
Experimental results	3.97	-0.17
P-TiO <sub>2</sub>		
Calculation results	2.80	-0.51
Experimental results	2.76	-0.53

Note: Absolute vacuum (E<sub>AVS</sub>) is 0 eV, and standard hydrogen electrode (E<sub>e</sub>) is 4.6 eV.

## References:

1. Lin, B.; Li, S.; Peng, Y.; Chen, Z.; Wang, X., MOF-derived core/shell C-TiO<sub>2</sub>/CoTiO<sub>3</sub> type

II heterojunction for efficient photocatalytic removal of antibiotics. *Journal of Hazardous Materials* **2021**, *406*, 124675.

2. Lu, Y.; Ding, C.; Guo, J.; Gan, W.; Chen, P.; Zhang, M.; Sun, Z., Highly efficient photodegradation of ciprofloxacin by dual Z-scheme Bi<sub>2</sub>MoO<sub>6</sub>/GQDs/TiO<sub>2</sub> heterojunction photocatalysts: mechanism analysis and pathway exploration. *Journal of Alloys and Compounds* **2022**, *924*, 166533.

3. Li, M.; Zhang, J.; Wang, L.; Cheng, X.; Gao, X.; Wang, Y.; Zhang, G.; Qi, Y.; Zhai, H.; Guan, R.; Zhao, Z., Direct Z-Scheme Oxygen-vacancy-rich TiO<sub>2</sub>/Ta<sub>3</sub>N<sub>5</sub> heterojunction for degradation of ciprofloxacin under visible light: Degradation pathways and mechanism insight. *Applied Surface Science* **2022**, *583*, 152516.

4. Wu, D.; Li, J.; Guan, J.; Liu, C.; Zhao, X.; Zhu, Z.; Ma, C.; Huo, P.; Li, C.; Yan, Y., Improved photoelectric performance via fabricated heterojunction g-C<sub>3</sub>N<sub>4</sub>/TiO<sub>2</sub>/HNTs loaded photocatalysts for photodegradation of ciprofloxacin. *Journal of Industrial and Engineering Chemistry* **2018**, *64*, 206-218.

5. Gherbi, R.; Nasrallah, N.; Amrane, A.; Maachi, R.; Trari, M., Photocatalytic reduction of Cr(VI) on the new hetero-system CuAl<sub>2</sub>O<sub>4</sub>/TiO<sub>2</sub>. *Journal of Hazardous Materials* **2011**, *186* (2), 1124-1130.

6. Wang, Y.; Kang, C.; Li, X.; Hu, Q.; Wang, C., Ag NPs decorated C-TiO<sub>2</sub>/Cd<sub>0.5</sub>Zn<sub>0.5</sub>S Z-scheme heterojunction for simultaneous RhB degradation and Cr(VI) reduction. *Environmental Pollution* **2021**, *286*, 117305.

7. Li, Y.; Liu, Z.; Wu, Y.; Chen, J.; Zhao, J.; Jin, F.; Na, P., Carbon dots-TiO<sub>2</sub> nanosheets composites for photoreduction of Cr(VI) under sunlight illumination: Favorable role of carbon dots. *Applied Catalysis B: Environmental* **2018**, *224*, 508-517.

8. Hu, X.; Zhao, Y.; Wang, H.; Cai, X.; Hu, X.; Tang, C.; Liu, Y.; Yang, Y., Decontamination of Cr(VI) by graphene oxide@TiO<sub>2</sub> in an aerobic atmosphere: effects of pH, ferric ions, inorganic anions, and formate. *Journal of Chemical Technology & Biotechnology* **2018**, *93* (8), 2226-2233.

9. Zhang, Z.; Huang, L.; Sheng, S.; Jiang, C.; Wang, Y., MIL-125(Ti)-derived COOH functionalized TiO<sub>2</sub> grafted molecularly imprinted polymers for photoelectrochemical sensing of ofloxacin. *Sensors and Actuators B: Chemical* **2021**, *343*, 130119.